The Outgoing Longwave Radiation Analysis of Medium and Strong Earthquakes

Bo Su, Hao Li, Weiyu Ma, Zhao Jing, Yao Qi, Cui Jing, Chong Yue, and Chunli Kang

***Abstract*—Two approaches are applied to outgoing longwave radiation (OLR) data to obtain abnormal changes before and after six earthquakes: the background field analysis (BFA) method, which focuses on statistically processing the increment of a radiation value to the multiyear average of the data; and the tidal force fluctuant analysis method, which abandons background data for many years by using the influence of tidal fluctuations to obtain incremental changes in radiation. The results demonstrate that the increase in OLR data identified via the BFA method was uncertain. In the time distribution, the occurrence time of anomalies is isolated and not continuous. In the spatial distribution, many OLR enhancement areas occurred multiple times in the nonseismic and remote seismic-related fault structure areas. In contrast, through the tidal force fluctuant analysis method a clear and consecutive OLR anomaly emerged in the seismogenic cycle of the tidal force. It corresponded with the tidal force through a unique evolution: increased-earthquake-shrink around the epicentre, consistent with the change in the law of thermal radiation during the rock-breaking process under stress, and clearly related to the earthquake's seismic tectonic stress change. It is proven that the tidal force of a celestial body may trigger an earthquake when the tectonic stress reaches its critical breaking point, and when the triggering action is a continuous rather than brief one-shot process. The *in situ* stress state is key. The OLR anomaly was the physical performance of underlying surface radiation from the change in seismic tectonic stress.**

***Index Terms*—Earthquake, outgoing longwave radiation (OLR) anomaly, thermal infrared, tidal force.**

I. Introduction

FOR more than 30 years, scholars from various countries have conducted thermal anomaly monitoring on a large number of seismic cases via satellite remote sensing, consequently claiming that the evolution in thermal anomalies in a seismic region reflects seismotectonic activities before and after an earthquake. Today, thermal infrared anomalies are generally classified under three main categories according to the implementation principle of each algorithm, with anomaly extraction based on either difference analysis [1], [2], signal analysis [3]–[6] or background field analysis (BFA) [7]–[10]. In the first type, the algorithm principle is simple, although it is necessary to combine other data in order to identify and interpret the extraction result, and it is difficult to eliminate the impact of short-term meteorological warming. The second case is also based on average change over time, covering short-term fluctuations in meteorological data, but explanation of its mechanism requires improvement. The third example, anomaly extraction based on the BFA, working through comparison with the background field for many years. it includes migration index algorithm of the same period over the years, RST algorithm, etc. The RST methodology identifies space-time anomalies always respect to a preliminarily defined "normal" (i.e., in unperturbed condition) signal behavior which is achievable by the analysis of long-term series of satellite records collected under similar observational conditions for each image pixel and period of the year [11], [12]. In the BFA method, the selection of background field mainly includes two kinds, namely, the mean of temperature in the same period of each year and the mean of temperature in the space domain [12]–[15]. But overall findings remain uncertain due to insufficient stability of the background field [16].

Due to the obvious influence of cloud in the atmosphere on infrared, Genzano *et al*. [17] used RST method to study the bright temperature anomaly before the earthquake and only calculated the cloud-free pixels, Tramutoli *et al.* [11], [18], Pergola *et al*. [15], did not calculate the pixels with clouds in the spatial computation, while Shao-Yan *et al*. [19] performed cloud removal on the bright temperature data before calculation. Zhang *et al*. [21] clearly proves that there are thermal anomalies under the cloud, and the operation of removing the cloud itself is wrong and should be handled with caution. The above arguments lead to question on the practicability and rationality of the RST method and the application range of bright temperature data. For if there are successively cloudy over the seismic genic area, the cloud removal, omit, replace and other operation will completely change the original radiation environment. How can the result reflect the infrared change before the earthquake? Therefore, it is necessary to find more practical and better data, and a means of selecting background data for the identification of thermal anomalies, as well as determine the period of thermal anomalies to be analyzed before an earthquake.

Manuscript received May 10, 2021; revised June 8, 2021; accepted June 14, 2021. Date of publication June 21, 2021; date of current version July 22, 2021. This work was supported in part by the National Key R&D Program of China, under Grant 2018YFC1503606, and in part by the APSCO Earthquake Project II: Integrating Satellite and Ground-Based Observation for Earthquake Precursors and Signatures. *(Corresponding author: Weiyu Ma.)*

Bo Su is with the School of Earth Sciences and Engineering, Hohai University, Nanjing 210098, China, and also with the School of Geography and Tourism, Nanyang Normal University, Nanyang 473061, China (e-mail: subohappy@hhu.edu.cn).

Hao Li is with the School of Earth Sciences and Engineering, Hohai University, Nanjing 210098, China (e-mail: lihao@hhu.edu.cn).

Weiyu Ma, Zhao Jing, Yao Qi, Chong Yue, and Chunli Kang are with the China Earthquake Networks Center, Beijing 100045, China (e-mail: weiyuma@163.com; zhaozhengjiajia1@126.com; yaoqi@seis.ac.cn; yuechong@seis.ac.cn; kangchli@seis.ac.cn).

Cui Jing is with the Institute of Crustal Dynamics, China Earthquake Administration, Beijing 100045, China (e-mail: cuijing@email.eqicd.cn).

Digital Object Identifier 10.1109/JSTARS.2021.3090777

TABLE I
LIST OF EARTHQUAKES IN THIS ANALYSIS [FROM USGS CATALOG (HTTPS://EARTHQUAKE.USGS.GOV/EARTHQUAKES/)]

Number	Name	Date (dd/mm/yyyy)	Epicentre location (°)	Magnitude (Mw)	Tectonic settings
1	Osaka, Japan	17/06/2018	34.843°N, 135.622°E	5.5	reverse fault
2	Tanabe, Japan	19/11/2016	33.814°N, 135.420°E	5.3	reverse fault
3	Greece	14/02/2008	36.5°N, 21.67°E	6.9	reverse fault
4	Turkey	23/10/2011	38.71°N, 43.52°E	7.2	strike slip
5	Xinjiang, China	08/03/2012	39.383°N, 81.307°E	5.9	strike slip
6	Oklahoma, USA	06/11/2011	35.532°N, 96.765°W	5.7	strike slip

An alternative form of pre-earthquake thermal identification based on tidal wave dynamics and the tidal force fluctuant analysis method has been utilized for some earthquakes. This method is an analytical method subtracting the normal background image from a series of temperature images according to the tidal force fluctuant cycles based on OLR data. This procedure is done in order to reduce disturbances from other factors and extract the abnormal temperature increase caused by activities in the Earth's crust [22], [23]. This algorithm does not require long-term background data and its thermal anomaly results are consistent with the law of thermal radiation change in the process of rock mechanics loading fracture, that is, increasing→strengthen→peak→fading→re-strengthen→calmness [22], [24]–[26].

In this article, we use anomaly extraction algorithms based on the BFA and the tidal force fluctuant analysis methods to identify thermal anomalies prior to the Osaka 2018 Mw5.5 earthquake, a Mw5.3 of 2016 earthquake in a similar location, and four other earthquakes (see Table I) on different continents with various seismotectonic and meteorological conditions and strengths (see Table I). We present the results of our analysis of outgoing longwave radiation (OLR) data obtained using these methods, and attempt to solve existing problems in thermal anomaly analysis before earthquakes.

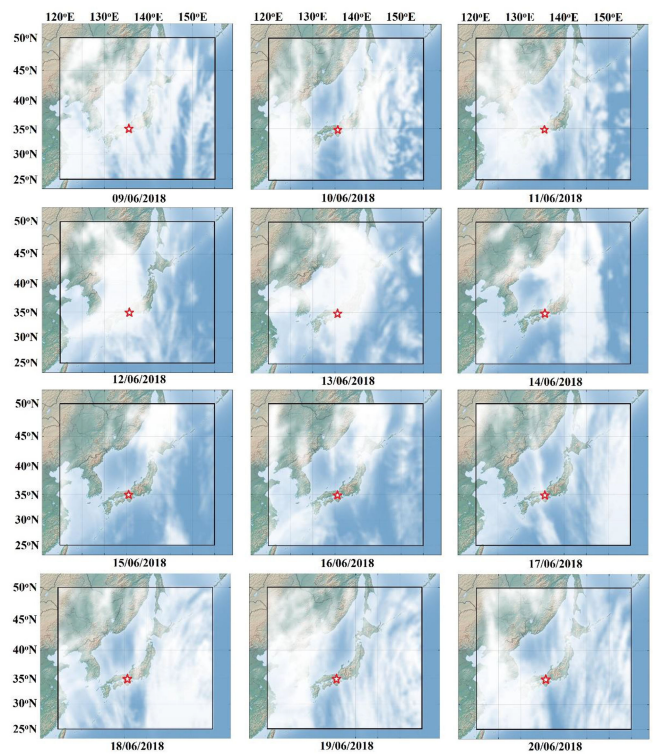

Fig. 1. Satellite cloud images from June 9–20, 2018, before and after the M5.5 Osaka earthquake of June 17, 2018 in Japan. The red five-pointed star is the epicenter.

II. DATA AND METHODOLOGY

A. Data

We chose OLR, which is the thermal radiation flux emergent from the top of the atmosphere and connected with the earth-atmosphere system in general, which is an unknown combination/convolution of the ground radiation, cloud radiation, absorption and radiation of the atmosphere, a function of atmospheric temperature and humidity profiles, and there is no need to remove cloud processing when studying the correlation with earthquakes. It has been applied to the analysis of seismic thermal anomalies by many scholars [27]–[30]. OLR is the heat radiation flux(W/m2) emerging from the upper atmosphere, widely used in the analysis of thermal anomalies before earthquakes [29], [31]–[33]. Here, we analyzed NOAA/AVHRR OLR data collected from the U.S. National Weather Service Environmental Modeling Center.[1]

[1]Online. [Available]: http://www.emc.ncep.noaa.gov

The NOAA OLR is the commonly used data product in various studies and is retrieved from the AVHRR TIR bands (10.5–12.5 μm) with daily and monthly mean values [34]. Given that the BFA method requires long-term background data, we use OLR data with a spatial resolution of 2.5° × 2.5°. In contrast, the tidal force fluctuant analysis method does not need long-term background data, allowing us to use a higher spatial resolution of 1° × 1°. The temporal resolution used by both methods is daily.

Cloud processing is an important issue in the identification of seismic thermal anomalies. To this end, we first analyzed the cloud status of the study area. The cloud map (see Fig. 1) of Osaka 2018 Earthquake was extracted, and it was found that there were a large number of clouds continued to exist for many days before the earthquake. If only cloud-free pixels are considered or

data is decloud processed, we will lose a large amount of the most critical infrared thermal information of impending earthquakes, and the relationship between the infrared parameters of reaction heat and earthquake could not be realized. Therefore, in order to more truly reflect the original radiation environment changes, we did not revise, remove or replace the data of the cloud period in the calculation. On the other hand, TIR data where there any clouds are totally influenced by the presence of the clouds. The effect is completely unknowable. If you include the cloudy pixels in your TIR analysis, the results are meaningless. So we did not use brightness temperature data.

B. BFA Method

The BFA method used in this article is the migration index algorithm based on the mean value of temperature in the same period over the years [10], [19]. This method is based on spatio-temporal analysis of several years of historical data sets for satellite observations obtained under identical observation conditions. It usually combines long-term series analysis of the epicentre with spatio-temporal analysis of the study area.

First, we collected the daily mean values of OLR one to two months before and after the earthquakes. The increment (ΔOLR) of a thermal parameter of each pixel on any day can be calculated as

$$\Delta OLR\ (r_i,\ t) = \mathrm{OLR}\,(r_i,\ t) - \frac{\sum \mathrm{OLR_{BY}}\,(r_i,\ t)\,E_{\mathrm{BY}}(r_i,\ t)}{E_{\mathrm{BY}}(r_i,\ t)}. \quad (1)$$

Where $\mathrm{OLR}(r_i,\ t)$ is the OLR value of the position r_i on any day t in the analysis time, $\mathrm{OLR_{BY}}(r_i,\ t)$ is the same pixel on the same day as $\mathrm{OLR}(r_i,\ t)$ in the background year we chose (the background year chosen in this article is 30 years). $E_{\mathrm{BY}}(r_i,\ t)$ is the marker value of pixel (r_i consistent with image acquisition time, BY is the background year. If there is no medium-to-large ($M > 5.5$) earthquake, $E_{\mathrm{BY}}(r_i,\ t) = 1$; otherwise, $E_{\mathrm{BY}}(r_i,\ t) = 0$

In time series analysis, we use $\Delta\mathrm{OLR}(r_i, t) > n * \delta(r_i)$ to identify anomalies. Where $\delta(r_i)$ is the standard deviation of $\delta(r_i)$ at the same position and at the same time for many years. Some researchers identified earthquakes using a threshold of 1 δ, some using 1.5 δ and some using 2 δ, 3 δ [7], [12], [34], and so on. In this study, we analyze the values of n = 1, 1.5, 2 respectively.

To observe the spatial relationship between the anomaly and the epicentre, we analyzed the spatial distribution of the OLR anomaly by calculating the anomaly index $K(r_i,\ t)$

$$K\,(r_i, t) = \frac{\mathrm{OLR}\,(r_i,\ t) - \mu\,(r_i)}{\delta\,(r_i)} \quad (2)$$

where $K(r_i,\ t)$ is the anomaly index value of the pixel at time t and position r_i; $\mathrm{OLR}(r_i,\ t)$ is the pixel value at time t and position r_i; $\mu(r_i)$ is the mean value at the same position and time for many years; and $\delta(r_i)$ is the corresponding standard deviation.

C. Tidal Force Fluctuant Analysis Method

The tidal force fluctuant analysis is a thermal anomaly extraction algorithm based on tidal force. It first calculates the change curve of tidal force in the epicentre over time, and then judges the phase of the tidal force-induced earthquake according to the structure of the seismic region. Next, the time of this phase is taken as the background time of OLR anomaly extraction in order to analyze the space-time sequence of OLR.

The tidal force induced by celestial bodies represents one of the most important external causes of ground stress, which may accumulate to the extent of triggering an earthquake [35]–[37]. It is periodically and continuously changing and the phase of its seismic induction varies with seismic structure [22], [38], [39]. At present, the tide-generating force of celestial bodies is the only earth deformation phenomenon that can be calculated in advance, which has a certain indicative function in the time domain, but it is difficult to judge whether the stress intensity of seismogenic tectonic movement will reach the critical point.

Subsequently, based on the tidal cycle, the starting time of each cycle was taken as the reference time background and the change in satellite OLR data was extracted according to (3). Generally, the starting phase of each cycle is the previous turning point of the phase of the earthquake, and the phase of the tidal force position at the time of the earthquake has a certain relationship with the type of earthquake. The normal fault and strike-slip type earthquake mostly occurs near the peak of the tidal force position. Usually, the first low-value phase moment before them is selected as the background moment, and then the moment is subtracted daily; the reverse fault type earthquake occurs mostly in the low tide position, and preseismic high point is usually chosen as the background of this period [21], [23]–[25].

Continuous changes in images before and after the earthquake were obtained as the basis to analyze impending seismic anomalies

$$\Delta\mathrm{OLR}_i\ (x, y) = \mathrm{OLR}_i\,(x, y) - \mathrm{OLR_{background}}\,(x, y) \quad (3)$$

Here, $\Delta\mathrm{OLR}_i(x, y)$ is the OLR incremental value of each grid point, $\mathrm{OLR}_i(x, y)$ is the OLR value of each grid point, and $\mathrm{OLR_{background}}(x, y)$ is the OLR value of the fixed background. In this article, we use the starting time of each cycle as the time background for the following cycle, and *x, y*, and *i* to denote the latitude, longitude and grid-point mark, respectively.

III. OLR Changes in Earthquakes in Japan Using the BFA and the Tidal Force Fluctulant Analysis

A. Case of the June 17, 2018 Osaka Earthquake

On June 17, 2018 at 07:58 UTC, a Mw 5.5 earthquake occurred 2 km NNW of Hirakata, Japan. The location of its epicentre was 34.843° N, 135.622 °E with a focal depth of 13 Km. The earthquake had the highest magnitude ever observed by the Japanese meteorological agency in Osaka, Japan, since the beginning of observation history in 1923. The seismic mechanism shows that the shock structure belongs to the reverse fault.

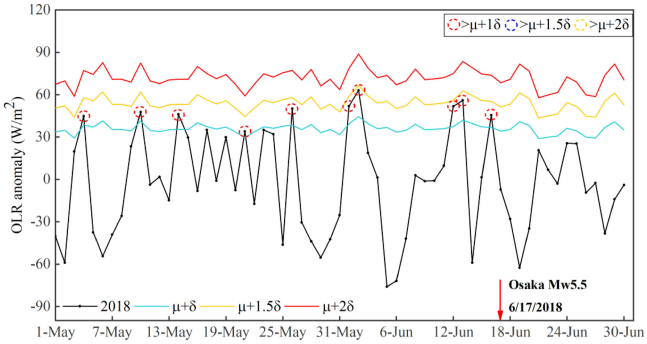

Fig. 2. Time series of daily OLR anomalies for May 1–June 30, 2018 at the epicentre of the M5.5 Osaka earthquake of June 17, 2018.

B. OLR Change of the Osaka Earthquake of June 2018 Using BFA

1) Result in Time: Fig. 2 displays the time series of daily OLR anomalies for May 1– June 30, 2018 at the epicentre (34.843° N, 135.622° E) of the Osaka earthquake. If we take $n = 1$, it can be seen that ten days were identified as anomalies in the OLR field, specifically May 4, May 10, May 14, May 21, May 26, June 1, June 2, June 12, June 13, and June 16. Of these dates, the ΔOLR value of June 2 reached the maximum of 63 W/m2. No earthquake occurred within 14 days afterwards. Moreover, no earthquake occurred within 14 days following an abnormal day other than June 12, June 13, and June 16. With so many anomalies, why were there no corresponding earthquakes? Even when anomalies occurred on June 12, June 13, and June 16—the days immediately preceding the June 17, earthquake—they were not the highest of all anomalies. How do we judge which anomaly indicates an upcoming earthquake? If we take $n = 1.5$, we can see that no anomaly is identified, let alone that n is larger.

2) Spatial Distribution: Fig. 3 displays the spatial distribution of the OLR anomaly in the research area before and after the Osaka earthquake. We use different colors to express different anomaly index K. The value of anomaly index greater than 1 and less than 1.5 is considered as weak anomaly, the value of anomaly index 1.5–2 is considered as slightly strong anomaly, and the value greater than 2 is considered as strong anomaly. There were some significantly abnormal OLR increases from May 12 to June 4. On May 12 an anomaly appeared in the northeast region far from the epicentre, with an anomaly index value of 2–2.2. On May 13, a slightly larger anomaly appeared in the northwest. On May 14 anomalies occurred in several places. The highest value (2.2) appeared in the southeastern part of the epicentre, while most other areas presented values of approximately 1.8. A weak anomaly of 1.6 occurred near the epicentre. Abnormal decreases were observed from May 15 to May 18. On May 19 the southern region, far from the epicentre of the earthquake, experienced anomalies and peaked at 2.5 from April 28 to April 30. On June 1 a weak anomaly (2.0) appeared at the epicentre and in most regions monitored. On June 2 the anomalous range grew and the anomalous region

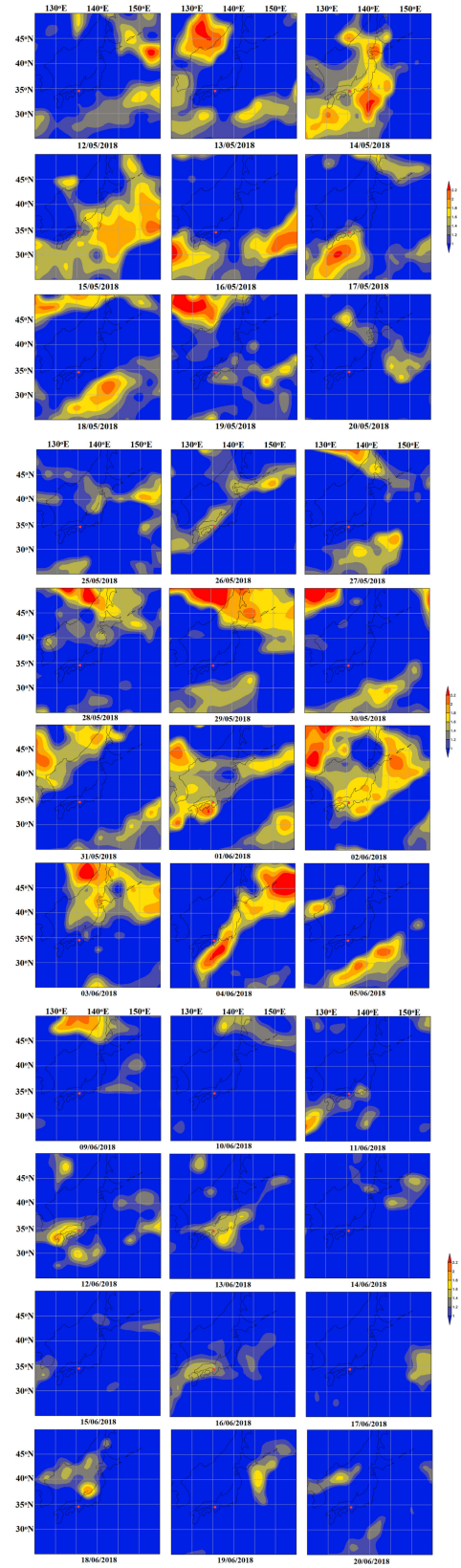

Fig. 3. Daily maps for May 12–June 20, 2018, representing the OLR anomalies' spatial extent over the M5.5 Osaka earthquake of June 17, 2018.

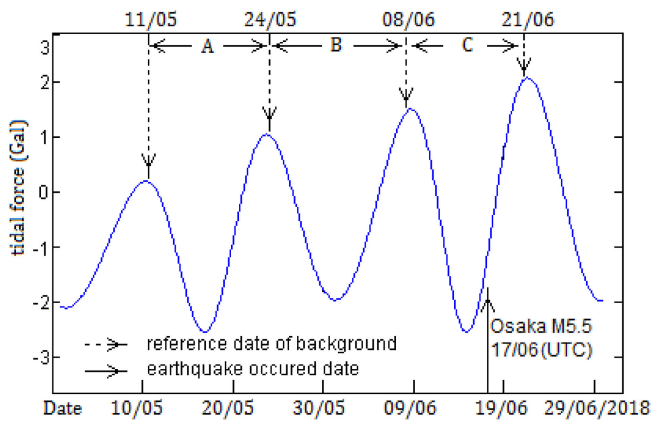

Fig. 4. Variations in tidal force from a celestial body before and after the Osaka M 5.5 earthquake.

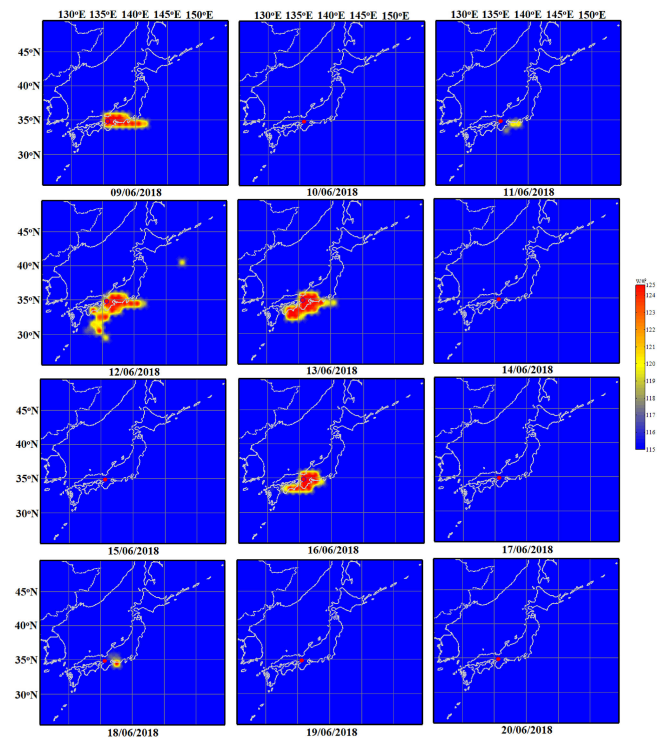

Fig. 5. Spatial-time evolution of the OLR of the Osaka (Japan) earthquake on 17 June 2018. Note: epicentre = •.

in the south was strengthened. On June 3 the anomalous region near the epicentre disappeared. On June 4 the anomalous region to the north of the epicentre was strengthened, with a value of 2.2. At the same time, a wide range of anomalies with values of 2.2 occurred in the northeast, far from the epicenter. As can be seen from these data, numerous regions demonstrated enhanced OLR, especially those far from the epicentre or seismically related fault structures. Moreover, only sporadic OLR enhancements occurred at the epicenter and in related regions, which were either large in area or extremely insignificant relative to the enhancement regions in general. We cannot distinguish which anomalies were related to earthquakes or as certain the locations of the earthquakes.

C. Tidal Force Change and OLR Data Processing of the Osaka Earthquake of June 2018

1) Tidal Force Change: The continuous change curve of the tidal force at the epicentre from May 1 to June 30, 2018—the same time period analyzed by the BFA method—is plotted in Fig. 4. The abscissa is the time series and the ordinate is the intensity of tidal force. The unit is Gal.

From May 11, 2018, the tidal forces of celestial bodies displayed three consecutive periods (A: May 11–23; B: May24–June 7; and C: June 8–21), continuous from peak → trough → peak, which were clearly cyclical changes. An earthquake (indicated by the arrow) occurred on June 17, 2018 (UTC), and the tidal force was in a trough phase. This suggests that the tectonically induced earthquake region was a reverse fault, consistent with the result of the focal mechanism solution, and thereby demonstrating that the tidal force has a certain evoked effect on the earthquake. However, visually showing the correlation between tidal change and tectonic stress change constitutes an issue that has vexed researchers for many years. Laboratory rock mechanics and loading experiments have revealed a general phenomenon: in the process of rock stress ruptures, the infrared radiation in the area of rupture shows a significant fluctuation process of increase→attenuation→enhancement →disappearance [40]–[48]. Although it is the result of the loading experiment in the laboratory, it provides us with an idea of macroidentification and whether there are similar phenomena in macro seismic observation, which is of great value for the identification of seismic thermal anomalies. For this purpose, we used ground OLR data to analyze the characteristics of regional radiation under different tidal cycles from macroscopic perspectives to indirectly reflect the relationship between stress changes and regional radiation.

2) Change Process of OLR Using the Tidal Force Fluctuant Analysis Method: In the case of the Osaka earthquake of June 17, 2018, we used the OLR data on May 11, 2018, May 24, 2018 and June 8, 2018, as the background for each period of the tidal force fluctuant analysis: A (May 11–23, 2018), B (May 24–June 7, 2018), and C (June 8–21, 2018), which were the peak phase of the corresponding periods of the tidal force fluctuant analysis. Then, the OLR values from May 11 to June 21 were subtracted from this OLR benchmark value for the same region. Thus, we obtained a series of OLR variations, shown in Figs. 5 –7. The OLR survey for June 9–20, 2018, cycle C of the tidal force of the celestial body (see Fig. 5) indicates that a significant change in OLR occurred around the epicentre before and after the earthquake in the study area. The anomaly appeared near the epicentre on June 9 and disappeared on June 10. On June 11 the anomaly appeared northeast of the epicentre; on June 12 abnormal enhancement occurred and spread to the epicentre; on June 13 further abnormal enhancement occurred; on June 14 and 15 the abnormality disappeared again; and on June 17 the main shock occurred. After the earthquake, the abnormality rapidly disappeared by June 19 and calm continued into June 20. The abnormal distribution and

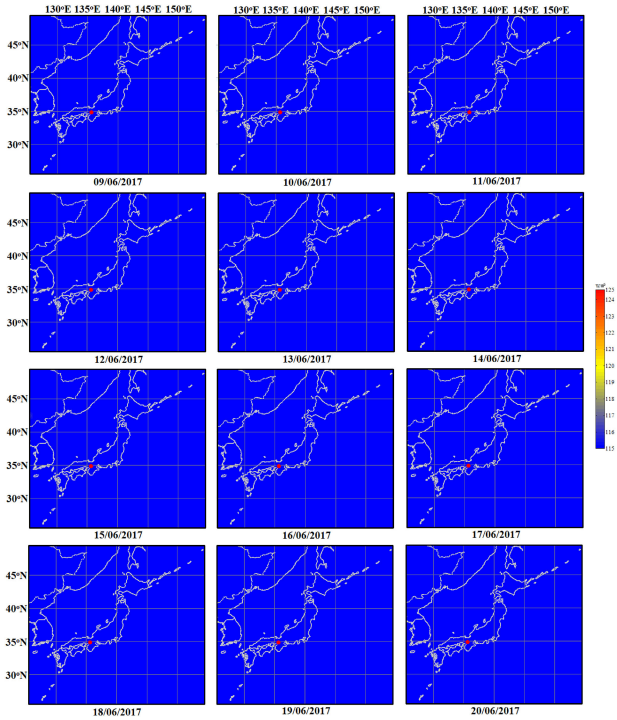

Fig. 6. Spatial-time evolution of the OLR of the Japan from June 9–20, 2017.

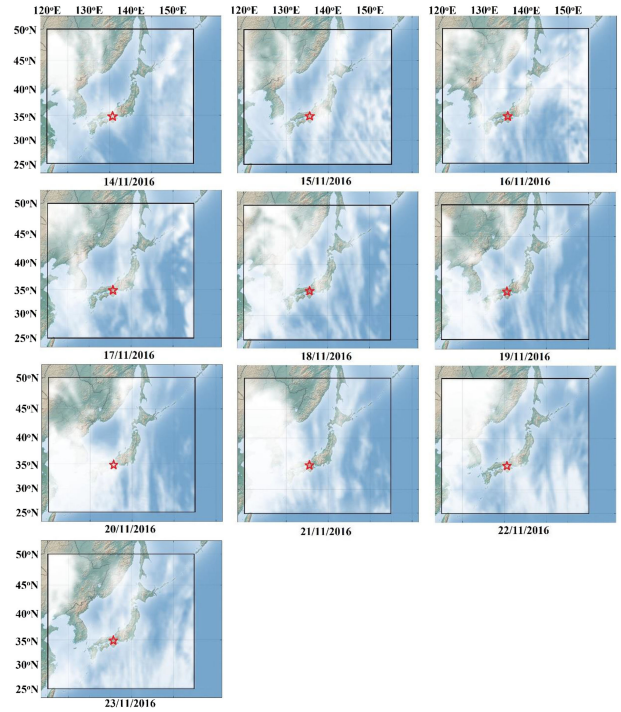

Fig. 7. Satellite cloud images from November 14–23, 2016, before and after the Mw 5.3 earthquake occurring 10 km NNE of Tanabe, Japan, on November 19, 2016. The red five-pointed star is the epicenter.

evolution of OLR had a strong correlation with the earthquake. Dispersion–convergence–dispersion–migration in the fault region was reflected in the OLR anomaly signal. Usually a change in OLR includes evolutions such as increasing → strengthen → peak → fading → re-strengthen → calmness, consistent with the rock failure process. The extrusion of tectonic movement comprises these evolutions: microbreaking→rupture strengthening → accumulating energy (the atresia of stress) → releasing energy → shaking → tranquilising [44]. Combining the cloud images during the earthquake period (see Fig. 1), clouds almost all existed over the epicenter during the OLR enhancement period, especially on the 13th when the radiation of the epicenter increased the most and the cloud coverage was also the strongest. Therefore, if cloud removal is done, the infrared changes during the earthquake period will be accurately eliminated.

However, in the same phase of the period of the tidal forces A (May 12–20 2018) and B (May 25–June 5, 2018), no significant OLR anomalies were found in this area. Therefore, no earthquake occurred. In addition, we analyzed the OLR in the same time period in 2017 and found that there were no earthquakes and no increase in OLR during this period (see Fig. 6).

D. OLR Analysis Using the Tidal Force Fluctuant Analysis With Another Earthquake Occurring in a Similar Location in Japan

To verify the reliability of the tidal force fluctuant analysis approach, we analyzed another Mw 5.3 earthquake, which occurred 10 km NNE of Tanabe, Japan on November 19, 2016 at 02:48 UTC. This earthquake exhibited similar parameters to the Osaka earthquake with regard to mechanism and location.[2] The results showed that although there are still a lot of clouds in the corresponding period of OLR evolution (see Fig. 7), the OLR anomaly evolution from this earthquake were also analogous (see Fig. 8). In space, they were almost distributed along the east-west direction of the epicentre. In time, the OLR presented increasing→strengthen→peak→fading→re-strengthen→calmness. it also shows that using OLR combined with the TFFT method, the pre-earthquake cloud has little influence on the results, while the de-cloud operation should be careful. Similarly, we analyzed the OLR for this time period in 2017, and there was still no earthquake and no OLR enhancement (see Fig. 9).

IV. Analysis of Other Earthquake Cases in Different Regions Using the BFA and the Tidal Force Fluctuant Analysis

In order to analyze whether similar thermal anomaly identification processes occurred in earthquakes in other parts of the world, we considered cases in Greece, Turkey, Xinjiang (China), and Oklahoma (USA). Our results were similar.

A. BFA Results

The time series of daily OLR anomalies at the epicentre of four earthquakes are plotted in Fig. 10. When is greater than 1 δ, we mark it with a red circle, and when is greater than 1.5 δ, we mark it with a blue circle. When 1 δ is taken as the threshold

[2]Online. [Available]: https://earthquake.usgs.gov/earthquakes/

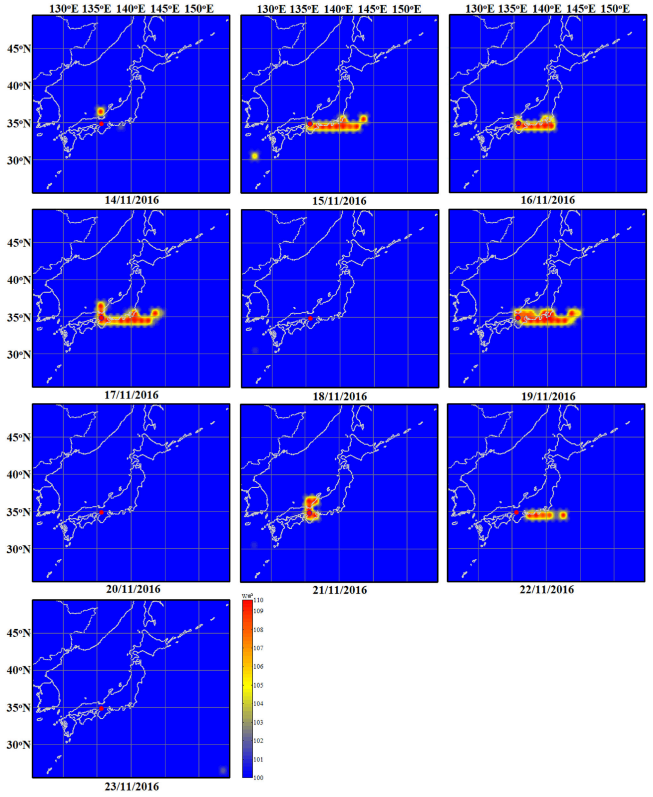

Fig. 8. Spatial-time evolution of the OLR anomaly increase from the Mw 5.3 earthquake occurring 10 km NNE of Tanabe, Japan, on November 19, 2016.

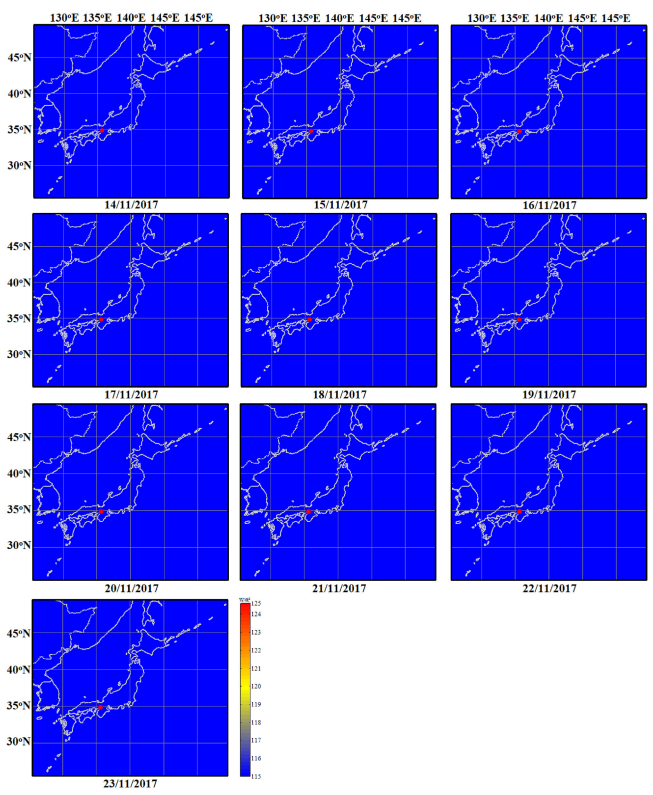

Fig. 9. Spatial-time evolution of the OLR of the Japan from November 14–23, 2017.

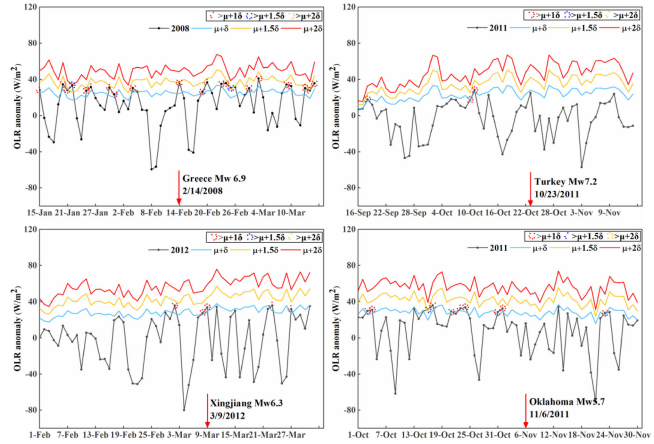

Fig. 10. Time series of daily OLR anomalies at the epicentre of the Greek, Turkey, Xinjiang, and Oklahoma earthquakes.

for anomaly recognition, it can be seen that these anomalies are numerous and scattered, and there is no corresponding earthquake behind the anomaly. Therefore, we cannot ascertain which anomaly indicates an upcoming earthquake. When taking 1.5 δ as the threshold for anomaly identification, the Turkey earthquake and Xinjiang earthquake did not identify anomalies. There were only two anomalies in the Greece earthquake, one was 23 days before the earthquake and one was 11 days after the earthquake. The Oklahoma earthquake only identified one anomaly, 21 days before the earthquake, so far away and isolated that we had no way of knowing if it was related to the earthquake. When taking 2 δ as the threshold, no anomalies were identified for all four earthquakes. Therefore, when the threshold of anomaly detection is small, the detected anomalies are many but scattered; when the threshold of anomaly detection is large, the detected anomalies are few, isolated and far away from the seismogenic time, and the detected anomalies do not follow certain rules. Therefore, it is difficult to determine the possible time of seismogenic time through infrared enhancement.

Given the limited space here, we only include some representative maps (images of anomalies near the epicenter and strong anomalies in the study area) to reflect the changes in OLR abnormalities in the study area over time (see Figs. 11–14). It can be seen that although these earthquakes all present anomalies near the epicentre, they sporadically jump; moreover, abnormalities away from the epicentre are stronger than those close by. Therefore, it is not particularly easy to distinguish which anomalies are related to earthquakes in the spatial distribution map of OLR anomalies obtained by the BFA method.

B. Tidal Force Fluctuant Analysis Results

Fig. 15 shows the tidal force change curves of the four earthquakes on different continents over time. The arrow refers to the earthquake time, while the vertical line is the background time of the seismic cycle. It can be seen that the celestial tidal force change is a continuous process with obvious periodicity, consistently presenting the cycle of trough→peak→trough→peak.

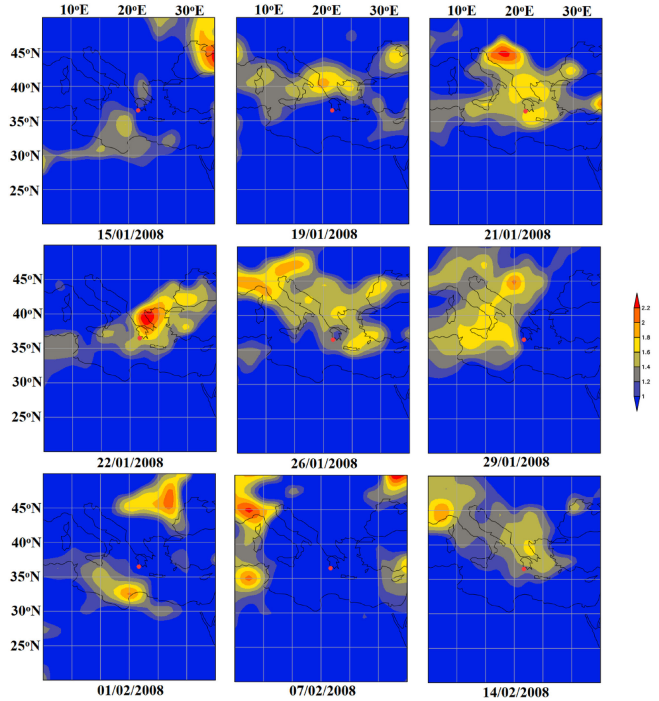

Fig. 11. OLR evolution in the spatial distribution of the Mw 6.9 Greece earthquake on February 14, 2008.

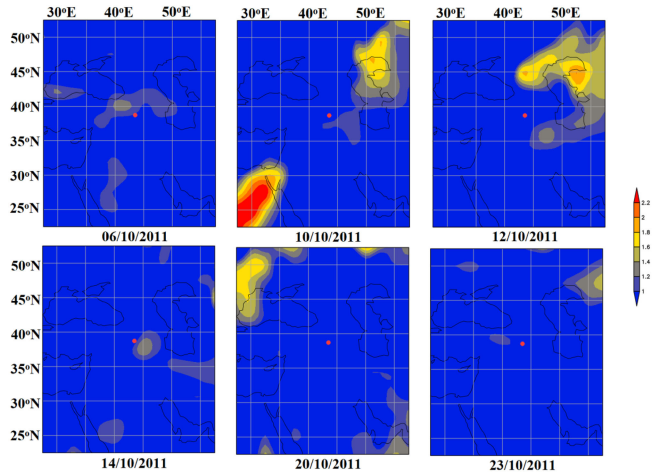

Fig. 12. OLR evolution in the spatial distribution of the Mw 7.2 Turkey earthquake on October 23, 2011.

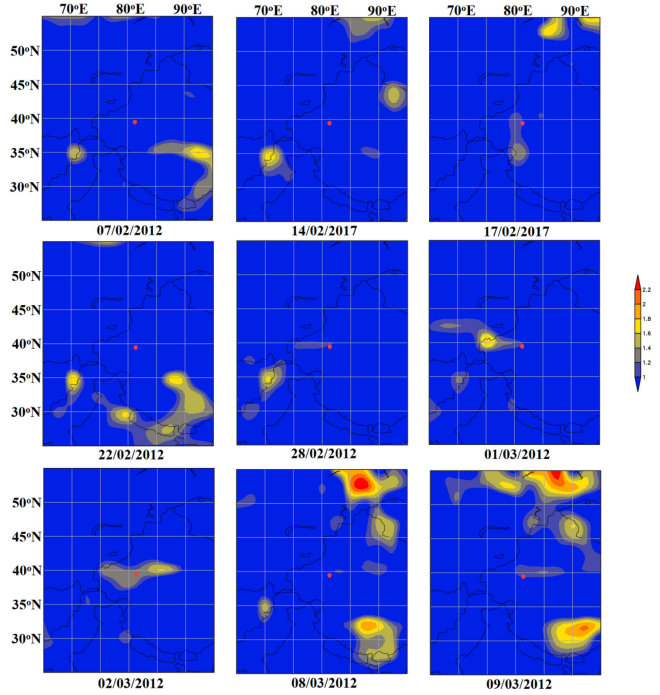

Fig. 13. OLR evolution in the spatial distribution of the Mw 5.9 Xinjiang earthquake on March 8, 2012.

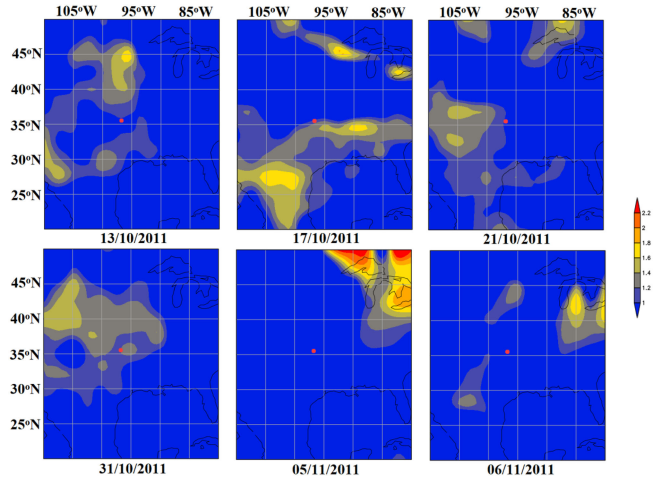

Fig. 14. OLR evolution in the spatial distribution of the Mw 5.7 Oklahoma earthquake on November 6, 2011.

Each turning point indicates that the celestial tidal force alters the nature of the tectonic environment to enhancement→ attenuation→ enhancement→ attenuation of the transformation process. Ma *et al*. pointed out that earthquakes occurring at the highest stage of tidal force had normal faults or approximately normal strike-slip faults with low background. The earthquakes that occur in the area of reverse fault tectonics mostly occur when the tidal force is low, and the background generally occurs when the tidal force is high [20]. Due to the diversity of tectonic settings, the earthquakes occurred at different periods of the tidal force of the celestial body, although all four took place after the tidal force was closest to the turning point, reflecting the continuous accumulation and strengthening of the stress. This indicates that the instantaneous change of the tidal force often fails to result in an earthquake, and its damaging effect on the seismic structural stress balance represents a continuous process.

To help verify the method's recognition rate, we zoomed in and expanded the study area to achieve a coverage of $40^{\circ} \times 40^{\circ}$. Similarly, based on the tidal cycle, we obtained the spatial-time evolution of the OLR before and after the four earthquakes. The results demonstrated that all four presented a clear, continuous enhancement area around the epicentre only in the seismogenic cycle among the three consecutive variation cycles of

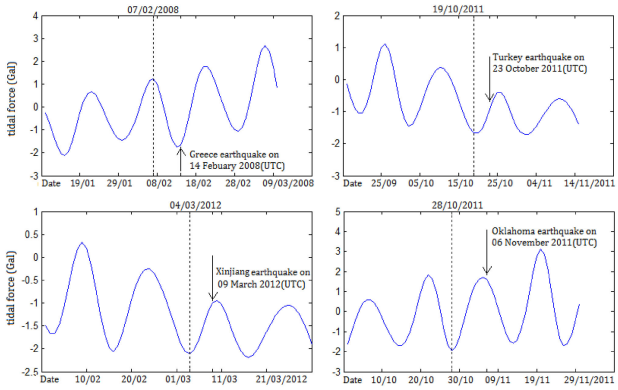

Fig. 15. Variations in tidal force from a celestial body before and after the Greece, Turkey, Xinjiang, and Oklahoma earthquakes. The vertical dashed line is the background time of the seismogenic cycle.

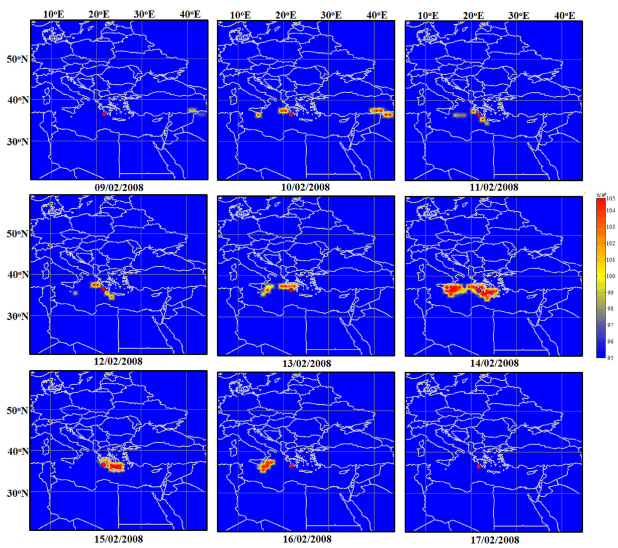

Fig. 16. Incremental field distribution of OLR of the Mw 6.9 Greece earthquake on February 14, 2008.

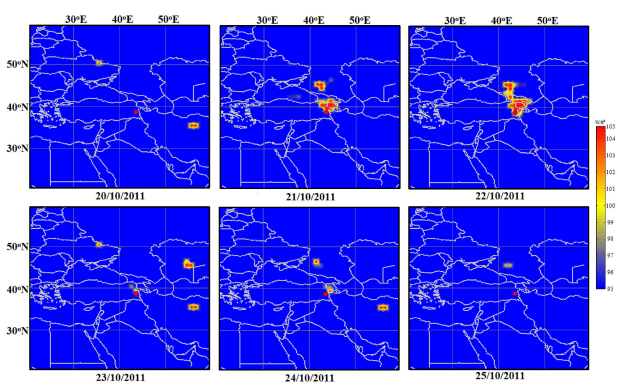

Fig. 17. Incremental field distribution of OLR of the Mw 7.2 Turkey earthquake on October 23, 2011.

the tidal force. And the highest point in the actual region, the region of continuous warming is the epicenter. In other tidal cycles, no significant OLR anomalies were identified and no earthquake occurred. Figs. 16–19 present the OLR temporal and spatial changes in the seismogenic cycle of the Greece,

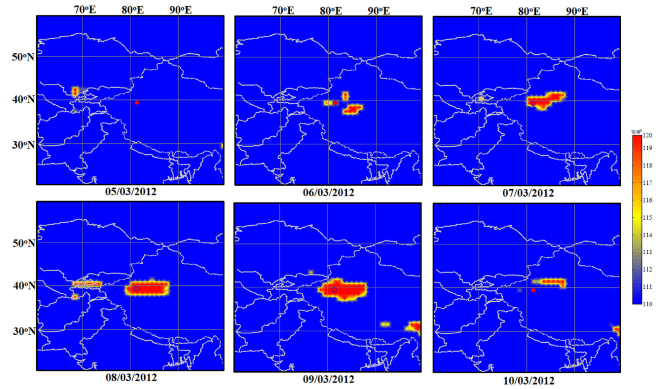

Fig. 18. Incremental field distribution of OLR of the Mw 5.9 Xinjiang earthquake on March 8, 2012.

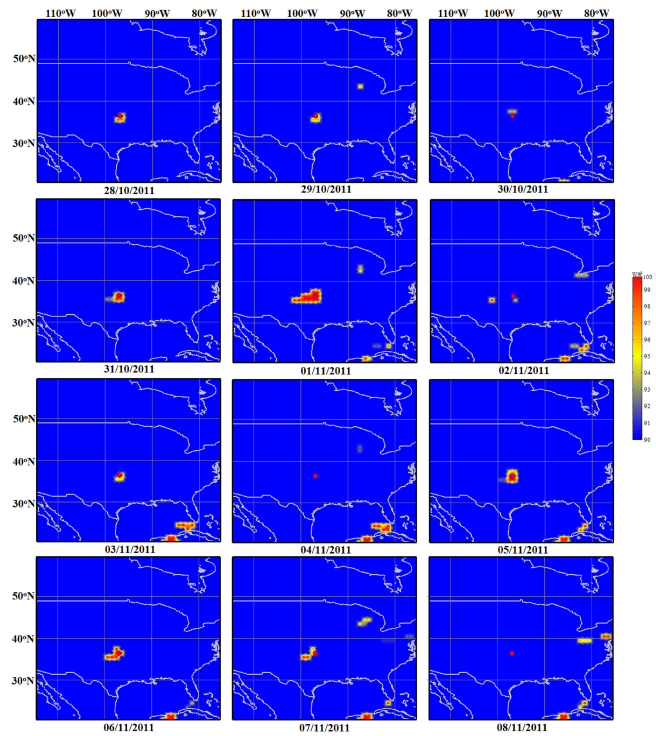

Fig. 19. Incremental field distribution of OLR of the Mw 5.7 Oklahoma earthquake on November 6, 2011.

Turkey, Sichuan and Oklahoma earthquakes, respectively. It can be seen that the enhancement demonstrated a similar evolution process (increase→ earthquake→ shrink around the epicentre), consistent with the rock failure process.

V. Discussion and Conclusion

The BFA and the tidal force fluctuant analysis methods were used to analyze the OLR changes before and after several earthquakes in different regions. Based on the BFA method, the OLR identification results of these earthquakes proved uncertain. In the time series analysis of anomaly recognition, we respectively take 1 δ , 1.5 δ and 2 δ for analysis, when taking 1 δ as the threshold, in the time series changes of OLR at

the epicentres of these earthquakes, many days were identified as abnormal, but no earthquake occurred during the follow-up period. Furthermore, the OLR variation on the day closest to the earthquake was not large. When the threshold was 1.5 δ, only a few anomalies were identified in the Oklahoma earthquake and Turkey earthquake. However, the occurrence date of the anomalies was more than 20 days apart from the time of the earthquake and it was isolated, so it was impossible to judge whether the anomalies were related to the earthquake. When 2 δ was taken as the threshold, all the earthquake examples in the article had no abnormalities identified. This may be that the seismic anomaly identification itself is to extract the weak signal under a strong background. The statistical method based on the BFA method depend on the availability of a large amount of historical data and is easily affected by various factors, lower threshold, will catch a lot of noise, improve the threshold, are undetectable. When the threshold is low, the abnormality cannot be identified correctly, and when the threshold is increased, the abnormality may not be found. In the spatial distribution, many OLR enhancement areas occurred multiple times in the nonseismic and remote seismic-related fault structure areas. Even if the OLR enhancement occurred sporadically near the epicentre, either the abnormal area was large or the abnormal amplitude was not prominent relative to the overall enhancement area. Moreover, the occurrence of anomalies was not continuous, which was inconsistent with the results of infrared radiation experiment of rock mechanics fracture. This renders it difficult to determine when and where earthquake-related anomalies will occur. In contrast, the OLR changes obtained using the tidal force fluctuant analysis method from the Osaka earthquake and another M5.3 earthquake with a similar location and physical mechanisms presented analogous abnormal characteristics. Moreover, the four earthquakes in other countries exhibited similar processes of evolution. During the study period, there was an obvious, continuous enhancement area near the epicentre. The enhancement near the epicentre was the highest in the whole image region. The enhancement represents the dynamic evolution of continuous increases before an earthquake and weakening afterward. This is akin to the thermal radiation evolution anomaly in the process of rock stress loading fractures, indicating that the evolution process is strongly correlated with earthquake formation. This process reflects the fact that the evolution process of the seismogenic tectonic environment in stress-strain fractures conforms to the continuous characteristics of stress microfracture rupture latching. It indicates that when the tectonic stress reaches its critical breaking point, the tidal force of the celestial body may trigger an earthquake, with the OLR anomaly the physical result of underlying surface radiation from the change in seismic tectonic stress. It is emphasized that the seismic thermal anomaly process is a continuous evolution process which is closely related to the seismogenic structure and conforms to the change law of rock rupture radiation under the action of stress, rather than a sporadic and irregular large-scale distribution.

It is also interesting to note that the magnitudes of the OLR anomalies in the six earthquakes differ, which should be related to the times at which the individual earthquakes occurred. The Osaka earthquake occurred in the summer, with high temperatures and the greatest increases. The Xinjiang earthquake occurred in the spring, and the temperature was relatively high, with a relatively large increase. The other four earthquakes occurred in the autumn or winter, with low temperatures and small increases. Finally, the OLR decay process prior to these earthquakes may have represented a sign of the lock-up period of rock stress. These findings may prove useful in detecting future earthquakes. In addition, we can see that the tidal force fluctuant analysis method in this article, the highest point in the actual region, the region with continuous warming is the epicenter, and several earthquake examples in this article are also reflected in this way. However, the existing research methods take n times sigma or specific values as the threshold to identify the anomaly, but the anomaly criteria defined by different methods and different earthquake cases are not consistent, which we believe is contradictory in itself. The earthquake itself is a process of energy accumulation to the outbreak, the pre-earthquake anomalies reflected in different earthquakes and different regions cannot be judged by quantitative data, but by the process of development before the earthquake.

As the only geophysical parameter that can be calculated in advance, tidal force not only provides predictable mechanical transformation indications for geophysical observations, but also offers a time component with clear mechanical implications for the remote sensing of anomalies. However, how the change in tidal force modulates and induces the occurrence of an earthquake and how the radiation anomaly is affected (especially under complex underlying surface conditions) is partially determined by non-seismic factors, such as topography, landform composition, and atmospheric circulation. The mechanism remains unclear. In future, it will be necessary to advance study of the physical mechanism of the tidal force seismogenic model and explore the precursory and recurrent characteristics of radiation anomalies in order to improve early warning ability prior to strong earthquakes in specific areas.

The fact of thermal radiation enhancement under cloud before earthquake and the processing results of different algorithms are presented in this article demonstrates that when using remote sensing technology to analyze the characteristics of phenomena, greater attention should be paid to the nature of the development and evolution of the phenomena themselves (or to their internal dynamic characteristics), rather than simply using statistical algorithms to examine problems.

References

[1] S. K. Panda, S. Choudhury, A. K. Saraf, and J. D. Das, "MODIS land surface temperature data detects thermal anomaly preceding 8 October 2005 Kashmir earthquake," *Int. J. Remote Sens.*, vol. 28, pp. 4587–4596, 2007.

[2] A. K. Saraf and S. Choudhury, "NOAA-AVHRR detects thermal anomaly associated with the 26 January 2001 Bhuj earthquake, Gujarat, India," *Int. J. Remote Sens.*, vol. 26, no. 6, pp. 1065–1073, 2005.

[3] M. R. Saradjian and M. Akhoondzadeh, "Thermal anomalies detection before strong earthquakes (M >6.0) using interquartile, wavelet and Kalman filter methods," *Natural Hazards Earth System Sci.*, vol. 11, no. 4, pp. 1099–1108, 2011.

[4] Y. S. Zhang, X. Guo, M. J. Zhong, W. R. Shen, W. Li, and B. He, "Wenchuan earthquake: Brightness temperature changes from satellite infrared information," *Chin. Sci. Bull.*, vol. 55, pp. 1917–1924, 2010.

[5] Z. Xuan, Z. Yuan-Sheng, W. Cong-Xin, T. Xiu-Feng, and F. Hong-Wu, "Thermal infrared anomaly prior to Yiliang of Yunnan MS5.7 earthquake," *China Earthquake Eng. J.*, vol. 35, no. 1, pp. 171–176, 2013.

[6] Z. Xuan, Z. Yuan-Sheng, W. Cong-Xin, T. Xiu-Feng, T. Qian, and G. Jian, "Analysis of thermal infrared anomaly before the Lushan M_S7.0 earthquake," *China Earthquake. Eng. J.*, vol. 35, no. 2, pp. 272–272, 2013.

[7] K. Qin, L. X. Wu, X. Y. Ouyang, X. H. Shen, and S. Zheng, "Surface latent heat flux anomalies quasi-synchronous with ionospheric disturbances before the 2007 pu'er earthquake in China," *Adv. Space Res.*, vol. 53, no. 2, pp. 266–271, 2014.

[8] W. Lixin *et al.*, "Geosphere coupling and hydrothermal anomalies before the 2009 mw 6.3 L'Aquila earthquake in Italy," *Natural Hazards Earth System Sci.*, vol. 16, no. 8, pp. 1859–1880, 2016.

[9] I. Mahmood, M. F. Iqbal, M. I. Shahzad, and S. Qaiser, "Investigation of atmospheric anomalies associated with Kashmir and Awaran earthquakes," *J. Atmospheric Sol.-Terr. Phys.*, vol. 60, no. 9, pp. 3457–3465, 2017.

[10] S. Ke, S. Xin-Jian, D. Ouzounov, S. Xu-Hui, and J. Feng, "Analyzing long wave radiation data associated with the 2015 Nepal earthquakes based on Multi-orbit satellite observations," *Chin. J. Geophys.*, vol. 60, no. 9, pp. 3457–3465, 2017.

[11] V. Tramutoli, "Robust satellite techniques (RST) for natural and environmental hazards monitoring and mitigation: Ten year of successful applications," in *9th Int. Symp. Phys. Meas. Signatures*, In Remote Sensing XXXVI (7/W20), pp. 792–795, 2005.

[12] N. Genzano, C. Aliano, R. Corrado, C. Filizzola, and V. Tramutoli, "RST analysis of MSG-SEVIRI TIR radiances at the time of the Abruzzo 6 April 2009 earthquake," *Natural Hazards Earth System Sci.*, vol. 9, no. 6, pp. 2073–2084, 2009.

[13] V. Tramutoli, V. Cuomo, C. Filizzola, N. Pergola, and C. Pietrapertosa, "Assessing the potential of thermal infrared satellite surveys for monitoring seismically active areas: The case of Kocaeli (Zmit) earthquake, August 17, 1999," *Remote Sens. Environ.*, vol. 96, no. 3-4, pp. 409–426, 2005.

[14] N. Genzano, C. Aliano, C. Filizzola, N. Pergola, and V. Tramutoli, "A robust satellite technique for monitoring seismically active areas: The case of Bhuj–Gujarat earthquake," *Tectonophysics*, vol. 431, no. 1–4, pp. 197–210, 2007.

[15] N. Pergola *et al.*, "Using RST approach and EOS-MODIS radiances for monitoring seismically active regions: A study on the 6 April 2009 abruzzo earthquake," *Natural Hazards Earth System Sci.*, vol. 10, no. 2, pp. 239–249, 2010.

[16] M. Blackett, M. J. Wooster, and B. D. Malamud, "Exploring land surface temperature earthquake precursors: A focus on the Gujarat (India) earthquake of 2001," *Geophys. Res. Lett.*, vol. 38, 2011, Art. no. L15303.

[17] N. Genzano, C. Filizzola, R. Paciello, N. Pergola, and V. Tramutoli, "Robust satellite techniques (RST) for monitoring earthquake prone areas by satellite TIR observations: The case of 1999 Chi-Chi earthquake (Taiwan)," *J. Asian Earth Sci.*, vol. 114, pp. 289–298, 2015.

[18] V. Tramutoli *et al.*, "On the possible origin of thermal infrared radiation (TIR) anomalies in earthquake-prone areas observed using robust satellite techniques (RST)," *Chem. Geol.*, vol. 339, pp. 157–168, 2013.

[19] W. Shao-Yan, Q. U. Chun-Yan, Y. Li-Li, S. Dong-Mei, and S. Xin-Jian, "Method for constructing regional brightness temperature background field and its preliminary aplication," *Earthquake*, vol. 31, no. 2, pp. 59–67, 2011.

[20] W. Ma, H. Zhao, and H. Li, "Temperature changing process of the Hokkaido (Japan) earthquake on 25 September 2003," *Natural Hazards Earth System Sci.*, vol. 8, pp. 985–989, 2008.

[21] X. Zhang, C. Kang, W. Ma, J. Ren, and Y. Wang, "Study on thermal anomalies of earthquake process by using tidal-force and outgoing-longwave-radiation," *Thermal Sci.*, vol. 22, pp. 153–153, 2017.

[22] W. Ma *et al.*, "Research on the changes of the tidal force and the air temperature in the atmosphere of Lushan (China) Ms7.0 earthquake," *Thermal Sci.*, vol. 19, pp. 148–148, 2015.

[23] W. C. Chen, W. Y. Ma, W. Ye, and H. F. Chen, "The research of the seismic objects of the tidal force and the temperature's change with Taiyuan's Yangqu Ms4.6," *Adv. Intell. Soft Comput.*, vol. 116, pp. 947–953, 2012.

[24] W. Y. Ma, H. Wang, F. S. Li, and W. M. Ma, "Relation between the celestial tide-generating stress and the temperature variations of the Abruzzo m = 6.3 earthquake in April 2009," *Natural Hazards Earth System Sci.*, vol. 12, no. 3, pp. 819–827, 2012.

[25] Z. Bo, L. Xuejun, and M. Weiyu, "The analysis of celestial tectonics-generating force's inducing effect to the M7.3 Japan earthquake on 9th, March 2011," *Procedia Environ. Sci.*, vol. 10, pp. 2005–2009, 2011.

[26] D. Ouzounov, D. Liu, K. Chunli, G. Cervone, M. Kafatos, and P. Taylor, "Outgoing long wave radiation variability from IR satellite data prior to major earthquakes," *Tectonophysics*, vol. 431, no. 1-4, pp. 211–220, 2007.

[27] K. Li and F. Liu, "The applicability of satellite remote sensing in monitoring earthquake," *Develop. Surv. Mapping*, vol. 26, no. 3, pp. 46–48, 2001.

[28] K. Chun-Li, L. De-Fu, C. Yan, and Z. Xiao-Cheng, "Research on earthquake prediction method in north china using outgoing-longwave-radiation information," *Northwestern Smolog. J.*, vol. 28, no. 1, pp. 59–63, 2006.

[29] D. F. Liu, "Abnormal detection on satellite remote sensing OLR before chichi earthquakes," *Geo-Inf. Sci.*, vol. 2, no. 1, pp. 33–36, 2000.

[30] F. Jing, X. Shen, C. Kang, Q. Meng, and S. Hong, "Extracting seismic anomalies based on STD threshold method using outgoing longwave radiation data," in *Proc. IEEE Int. Geosci. Remote Sens. Symp.*, 2010, pp. 1561–1564.

[31] F. Jing, X. Gu, and X. Shen, "Study on outgoing longwave radiation variations associated with strong earthquake," *Proc. SPIE Int. Soc. Opt. Eng.*, vol. 7651, pp. 765113, 2010.

[32] P. Xiong, Y. Bi, and X. Shen, "Study of outgoing longwave radiation anomalies associated with two earthquakes in China using wavelet maxima," in *Proc. Int. Conf. Hybrid Artif. Intell. Syst.*, 2009, pp. 77–77–87.

[33] A. Gruber and A. F. Krueger, "The status of the NOAA outgoing longwave radiation data set," *Bull. Amer. Meteorolog. Soc.*, vol. 65, no. 9, pp. 958–962, 1984.

[34] D. Ouzounov, N. Bryant, T. Logan, S. Pulinets, and P. Taylor, "Satellite thermal IR phenomena associated with some of the major earthquakes in 1999–2003," *Phys. Chem. Earth*, vol. 31, no. 4–9, pp. 154–163, 2006.

[35] T. H. Heaton, "Tidal triggering of earthquakes," *Geophys. J. Roy. Astronomical Soc.*, vol. 43, no. 2, pp. 307–326, 1975.

[36] S. Tanaka, M. Ohtake, and H. Sato, "Spatio-temporal variation of the tidal triggering effect on earthquake occurrence associated with the 1982 South Tonga earthquake of mw 7.5," *Geophys. Res. Lett.*, vol. 29, no. 16, pp. 3-1–3-4, 2002.

[37] S. Tanaka, "Tidal triggering of earthquakes prior to the 2011 Tohoku-Oki earthquake (Mw 9.1)," *Geophys. Res. Lett.*, vol. 39, no. 7, pp. L00G26 1-4, 2012.

[38] W. Y. Ma, H. Wang, F. S. Li, and W. M. Ma, "Relation between the celestial tide-generating stress and the temperature variations of the Abruzzo m = 6.3 earthquake in April 2009," *Natural Hazards Earth Syst. Sci.*, vol. 12, no. 3, pp. 819–827, 2012.

[39] Z. Jing, X. I. Qin-Wen, Y. Lin-Zhang, and C. Rong-Hua, "A study on tidal force/stress triggering of strong earthquakes," *Chin. J. Geophys.*, 2007.

[40] L. Wu and J. Wang, "Infrared radiation features of coal and rocks under loading," *Int. J. Rock Mechanics Mining Sci.*, vol. 35, no. 7, pp. 969–976, 1998.

[41] L. Wu, C. Cui, N. Geng, and J. Wang, "Remote sensing rock mechanics (RSRM) and associated experimental studies," *Int. J. Rock Mechanics Mining Sci.*, vol. 37, no. 6, pp. 879–888, 2000.

[42] L. Wu, S. Liu, Y. Wu, and H. Wu, "Changes in IR with rock deformation," *Int. J. Rock Mechanics Mining Sci.*, vol. 39, no. 6, pp. 825–831, 2002.

[43] L. X. Wu, S. J. Liu, Y. H. Wu, and J. Z. Wang, "FRM qualitative to quantitative: The development of remote sensing rock mechanics (RSRM)," *Int. J. Rock Mechanics Mining Sci.*, vol. 41, no. 1, pp. 310–316, 2004.

[44] L. Wu, S. Liu, Y. Wu, and C. Wang, "Precursors for rock fracturing and failure—Part I: IRR image abnormalities," *Int. J. Rock Mechanics Mining Sci.*, vol. 43, no. 3, pp. 473–482, 2006.

[45] L. Wu, S. Liu, Y. Wu, and C. Wang, "Precursors for rock fracturing and failure—Part II: IRR T-Curve abnormalities," *Int. J. Rock Mechanics Mining Sci.*, vol. 43, no. 3, pp. 483–493, 2006.

[46] L. Wu *et al.*, "Geosphere coupling and hydrothermal anomalies before the 2009 mw 6.3 L'Aquila earthquake in Italy," *Natural Hazards Earth System Sci.*, vol. 16, no. 8, pp. 1859–1880, 2016.

[47] F. Freund, "Time-resolved study of charge generation and propagation in igneous rocks," *J. Geophys. Res., Solid Earth*, vol. 105, no. B5, pp. 11001–11019, 2000.

[48] F. T. Freund, A. Takeuchi, B. W. S. Lau, A. Al-Manaseer, and D. Ouzounov, "Stimulated infrared emission from rocks: Assessing a stress indicator," *Earth*, vol. 2, no. 1, pp. 7–16, 2006.

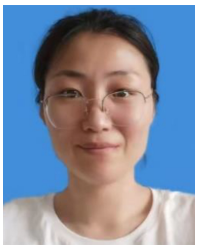

Bo Su received the M.S. degree from Hohai University, Nanjing, China, in 2011. She is currently working toward the Ph.D. degree in photogrammetry and remote sensing at Hohai University, Nanjing, China.

Her research interests include seismic thermal anomaly monitoring and geohazards perception and cognition.

Hao Li received the Ph.D. degree in 2005 from Hohai University, Nanjing, China,

He is currently a Professor with Hohai University, mainly engaged in teaching and scientific research in the direction of photogrammetry and remote sensing.

Weiyu Ma received the Ph.D. degree from Zhejiang University, Hangzhou China in 2006.

He is currently with China Earthquake Networks Center, Beijing, China. His research interests include remote sensing technology and application and earthquake precursor analysis.

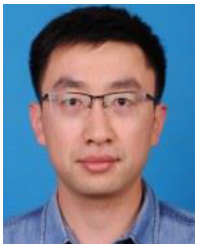

Zhao Jing received the Ph.D. degree from the Institute of Geology, China Earthquake Administration, Beijing, China, in 2021.

He is currently with China Earthquake Networks Center, Beijing, China. His research interests include crustal tectonic deformation, fault locking and post-seismic healing process.

Yao Qi received the Ph.D. degree from Zhejiang University, Hangzhou, China, in 2008.

She is currently with the Institute of Earthquake Forecasting, China Earthquake Administration. Her research interests include seismogenic structure modeling and related FEM simulation.

Cui Jing received the Ph.D. degree in earth exploration and information technology, China University of Geosciences, Beijing, China, July, 2014.

In 2019, she was an Associate Researcher with the National Institute of Natural Hazards, MEMC. Her research topics include remote sensing technology and application, active tectonics research, and earthquake precursor analysis.

Chong Yue is currently working toward the Ph.D. degree with the Key Laboratory of Earthquake Dynamics, Institute of Geology, China Earthquake Administration, Beijing , China.

He is currently an Assistant Researcher with China Earthquake Networks Center. His major is the solid earth geophysics, and the main research direction is the crustal deformation.

Chunli Kang received the B.S. degree from the Hebei Institute of Geology, Hebei, China, in 1987.

She is currently with Earthquake Networks Center, Beijing, China. Her research interests include seismic thermal anomaly monitoring and geohazards perception and cognition.